

Modified Chopper with Asymmetrical Control Strategy for High Power Applications

Vaka S Sandeep Kumar Reddy ¹

M-tech Student Scholar

Department of Electrical & Electronics Engineering,
BV RAJU INSTITUTE OF TECHNOLOGY, NARSAPUR;
MEDAK (Dt); Telangana, India.

MR. K. Ramakrishna ²

Associate Professor

Department of Electrical & Electronics Engineering,
BV RAJU INSTITUTE OF TECHNOLOGY, NARSAPUR;
MEDAK (Dt); Telangana, India

Abstract - In this paper an asymmetrical duty cycle control strategy was proposed to the TPTL dc/dc converter. The modified converter remains all the advantages of original control strategy; meanwhile, soft-switching can be achieved using the energy stored in output filter inductance and leakage inductances of transformers (or resonant inductances). Three-phase three-level (TPTL) dc/dc converter has the advantages of lower voltage and current stress on switches, which is suitable for high power and high input voltage applications. Adopting a symmetrical control strategy, the ripple frequency of input and output current can be increased significantly, resulting in a reduced filter requirement. To further reduce the current stress on switches for higher power. The improved resonant converter features zero-voltage-switching (ZVS) realization under wide load range and higher conversion efficiency. The proposed concept can be implemented with five level topology using Matlab/simulink software.

I. INTRODUCTION

Over the years single phase full-bridge (FB) and three-phase FB pulsewidth modulation (PWM) dc to dc soft switched converters have become popular in the field of dc to dc conversion system. For these converters metal oxide semiconductor field effect transistors (MOSFETs) are generally preferred over insulated gate bipolar transistors (IGBTs), because they can be operated at higher switching frequency and they do not have the problem of long tail current. However, these FB PWM soft switched converters are not suitable for switch mode power supply applications, where the input voltage is high. This is because the MOSFETs have to sustain high input dc link voltage. Moreover, service of auxiliary circuits is required to operate devices in soft switched mode. This requires extra components, devices and hence it leads to incurring additional cost while reducing the system reliability. In order to reduce the voltage stress to half of the input dc voltage, a three-level topology has been considered in [1] and [2] for inverter application and it has been used for realizing a dc to dc converter in [3]–[5]. The soft commutation is achieved by using phase shift PWM modulation [4], [5] which is having simple control structure and high power density can be achieved. However at high power levels, these components experience considerable current stress. In order to overcome this problem, topologies consisting of three-phase inverter coupled to a three-phase high frequency transformer followed by three-phase high frequency bridge-rectifier have been proposed [6]–[9]. This results in an increase in the input current and output current frequencies by a factor of

three as compared to the full bridge converter. This also results in lower current rating for the components and also a considerable reduction in size for the isolation transformer. However, the devices experience high voltage stress and the control structure is also quite involved. In an effort to overcome the aforementioned limitations a new converter topology involving three-phase, three-level, (TPTL) phase shifted PWM converter involving six switches operating as zero voltage switching (ZVS) and six switches operating as zero current switching (ZCS) has been presented in this paper. It should be mentioned that in this case soft switching of the semiconductor devices is achieved without taking help from any additional auxiliary circuitry comprising of active or passive elements. In the proposed topology the output rectifier is a center tapped full wave current tripler [10], [11] producing either two or three-level output voltage depending on the operating duty cycle. This leads to considerable reduction in size of the output filter compared to that of the conventional full bridge topology.

II. MODIFIED TPTL CONVERTER AND ASYMMETRICAL DUTY CYCLE CONTROL

Fig.1 shows the circuit configuration of TPTL converter in [19], in which, a three-phase transformer with Δ -Y connection is employed for the smaller turns ratios and transformer VA rating [20]. As shown, L_{ra} , L_{rb} and L_{rc} are the additional resonant inductances to widen the ZVS commutation load range. L_{lka} , L_{lkb} , and L_{lkc} are the equivalent primary leakage inductances of each phase. $Df1$ and $Df2$ are freewheeling diodes. C_{ss} is the flying capacitor, which is in favor of decoupling the switching transition of Q_1, Q_3, Q_4 , and Q_6 . $DR1$ – $DR6$ are rectifier diodes. The output filter is composed of L_f and C_f , and R_{Ld} is the load.

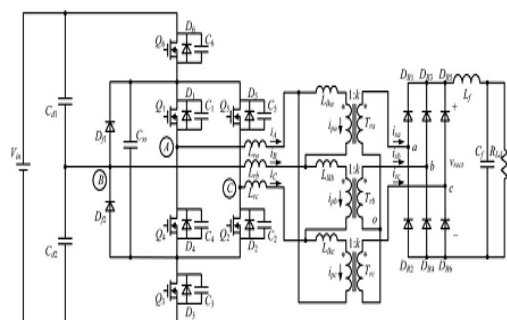
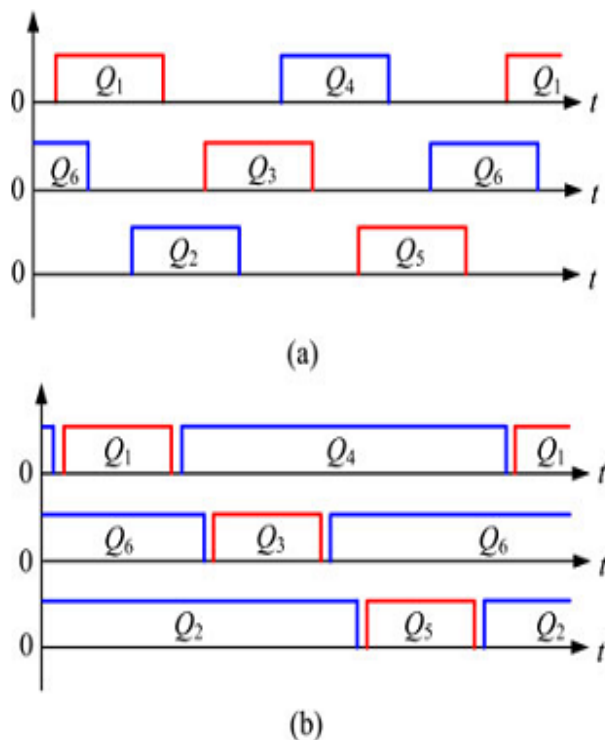


Fig.1. Topology configuration of TPTL dc/dc converter.

Fig.2 shows the switching sequences of the original control strategy and the modified control strategy, as shown in Fig. 2(a), Q1–Q6 are switched on in turn with interval of one-sixth switching period, the duty cycles of all switches are equal, and each switch has a maximum conduction period of 120°. The required range for the duty cycle of any switch is from 0.167 to 0.33. Obviously, the two interleaved switches have a simultaneous turn-off interval, during which, the intrinsic capacitors of two switches will resonate with the leakage inductances of transformers for several periods. As the duty cycle of the switches varies with the input voltage and the load, the incoming switch cannot be ensured to turn on exactly when its drain-to-source voltage resonates to zero within the operation range; therefore, the switches suffer hard-switching and a considerable switching loss occurs. To realize the soft-switching for switches, the original interleaved switches should be designed in a complementary manner, and a short delay time t_d is necessary to be introduced between the two complementary switches to provide an interval for the ZVS commutation, which is similar to the control strategy of asymmetrical half-bridge converter. Accordingly, the duty cycles of Q1, Q3, and Q5 are served to regulate the output voltage, while the drive signals of Q4, Q6, and Q2 are complementary to that of the Q1, Q3, and Q5, respectively. The obtained control strategy is illustrated in Fig. 2(b).

Fig. 2. Two kinds of control strategies of TPTL converter. (a) Symmetrical duty cycle control. (b) Asymmetrical duty cycle control.



III. OPERATION PRINCIPLE

This section will analyze the operation principles of the TPTL converter under the modified control scheme. The following assumptions are made for the simplicity before the analysis:

- 1) all power devices and diodes are ideal;
- 2) all capacitors and inductances are ideal;
- 3) the output filter inductance is large enough to be treated as a constant current source during a switching period; its value equals to output current I_o ;
- 4) the inductances of each phase are identical, i.e., $L_{lka} = L_{lkb} = L_{lkc} = L_{lk}, L_{ra} = L_{rb} = L_{rc} = L_r$;
- 5) $C_1 = C_2 = C_3 = C_4 = C_5 = C_6 = C_p$.

Fig. 3 shows the key waveforms of the TPTL converter with asymmetrical duty cycle control, as seen, the operation of the TPTL converter can be classified by different modes, according to the duty cycle range and the load current. The corresponding operation modes are defined as the small duty cycle mode (SDCM), the medium duty cycle mode (MDCM), and the large duty cycle mode (LDCM), respectively, when the duty cycle varies between (0, 1/3), (1/3, D_r), and (D_r , 1/2), where D_r is a critical duty cycle that depends on the load current and the parameters of converter. The related waveforms in different operation modes are referred to Fig. 3(a)–(c). For simplicity, only the operation principle under SDCM will be described in this paper. As shown in Fig. 3(a), the converter has 18 operation stages during a switching period.

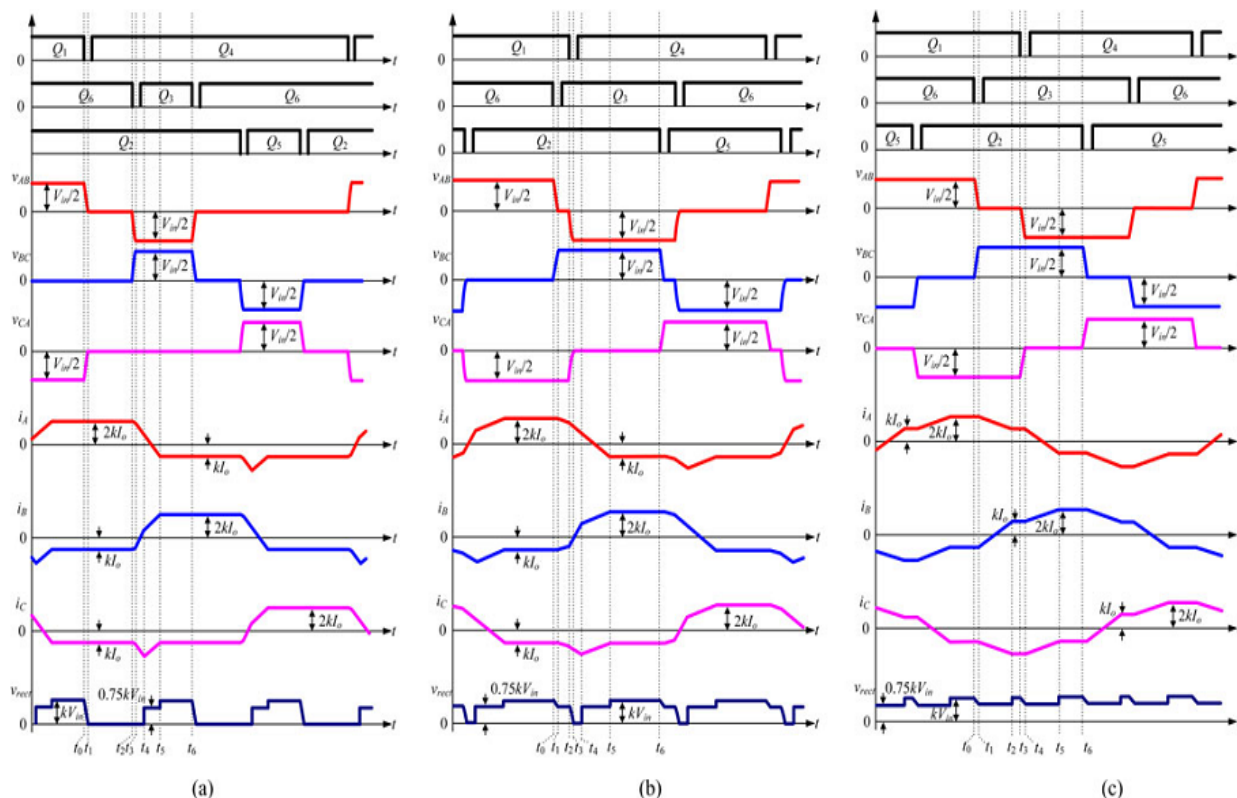


Fig.3. Key waveforms of the TPTL converter with asymmetrical duty cycle control. (a) SDCM. (b) MDCM. (c) LDCM

Fig. 4 shows seven operation stages of the converter under rated conditions. The other operation stages during the rest of a switching period are not depicted but they are symmetrically equivalent, except for the fact that they are phase shifted.

The basic equations of the voltages and currents of the transformer are listed as follows:

$$v_{AB} + v_{BC} + v_{CA} = 0 \tag{1}$$

$$i_{sa} + i_{sb} + i_{sc} = 0 \tag{2}$$

$$\begin{aligned} \frac{di_{pa}}{dt} &= k \frac{di_{sa}}{dt} = \frac{v_{Llka}}{L_{lk}}, \quad \frac{di_{pb}}{dt} = k \frac{di_{sb}}{dt} \\ &= \frac{v_{Llkb}}{L_{lk}}, \quad \frac{di_{pc}}{dt} = k \frac{di_{sc}}{dt} = \frac{v_{Llkc}}{L_{lk}} \end{aligned} \tag{3}$$

Where k represents the secondary-to-primary turns ratios of the transformer. The voltage across the leakage inductance of transformer can be derived from (2) and (3) and is given as follows:

$$v_{Llka} + v_{Llkb} + v_{Llkc} = 0. \tag{4}$$

Stage1 [prior to t_0] [see Fig. 3.4(a)]: Prior to t_0 , Q_1 , Q_2 , Q_6 , and D_{r2} are conducting at the primary side, and $DR1$ and $DR6$ are conducting at the secondary side. $v_{AB} = V_{in}/2$, $v_{BC} = 0$, and $v_{CA} = -V_{in}/2$. From (1), (2), (4), and other constraints between voltages and currents of transformers, the following expressions can be obtained:

$$v_{pa} = \frac{V_{in}}{2}, \quad v_{pb} = 0, \quad v_{pc} = -\frac{V_{in}}{2} \tag{5}$$

$$v_{rect} = v_{sa} - v_{sc} = k \cdot V_{in} \tag{6}$$

Where v_{pi} and v_{si} are the primary voltage and secondary voltage of transformers, I represents the subscripts a , b , and c .

Stage 2 [t_0, t_1] [see Fig. 4(b)]: At t_0 , Q_1 is turned off, the line current i_A charges C_1 and discharges C_4 linearly, and the rectified voltage decreases. As C_1 limits the rising rate of the voltage across Q_1 , Q_1 is zero-voltage turn-off. The voltages across C_1 and C_4 are

$$v_{C1}(t) = \frac{1}{C_p} \cdot k \cdot I_o \cdot (t - t_0) \tag{7}$$

$$v_{C4}(t) = \frac{V_{in}}{2} - \frac{1}{C_p} \cdot k \cdot I_o \cdot (t - t_0) \tag{8}$$

At t_1 , v_{C1} rises to $V_{in}/2$, and v_{C4} decays to zero; therefore, D_4 conducts naturally, and v_{rect} decreases to zero.

Stage3 $[t_1, t_2]$ [see Fig. 4(c)]: After C_1 is fully charged, the current flowing through C_1 transfers to C_{ss} and begins to charge C_{ss} . The voltage across C_{ss} will increase and block $Df2$ to be off. During this stage, $v_{AB}=v_{BC}=v_{CA}=0$. D_4 conducts and clamps the voltage across Q_4 at zero, so Q_4 can be turned on at zero-voltage condition. D_{R1} and D_{R6} conduct, and v_{rect} is still zero.

Stage4 $[t_2, t_3]$ [see Fig. 4(d)]: At t_2 , Q_6 is zero-voltage turned-off, and v_{AB} increases reversely. If v_{pa} keeps constant, the polarity of the voltage applied on L_{lk} will be non associated with the current flowing through L_{lk} ; as a result, i_{pa} will decrease and cannot provide the load current, then $DR3$ begins to conduct, and the current commutation between $DR1$ and $DR3$ occurs. In the primary stage, $C3$ and $C6$ resonate with the leakage inductances and the resonant inductances, and the following expressions will be obtained:

$$v_{C3}(t) = \frac{V_{in}}{2} - \frac{1}{2}k \cdot I_o \cdot Z_r \cdot \sin[\omega_r(t - t_2)] \tag{9}$$

$$v_{C6}(t) = \frac{1}{2}k \cdot I_o \cdot Z_r \cdot \sin[\omega_r(t - t_2)] \tag{10}$$

$$i_A(t) = \frac{3}{2}k \cdot I_o + \frac{1}{2}k \cdot I_o \cdot \cos[\omega_r(t - t_2)] \tag{11}$$

$$i_B(t) = -k \cdot I_o \cdot \cos[\omega_r(t - t_2)] \tag{12}$$

$$i_C(t) = -\frac{3}{2}k \cdot I_o + \frac{1}{2}k \cdot I_o \cdot \cos[\omega_r(t - t_2)] \tag{13}$$

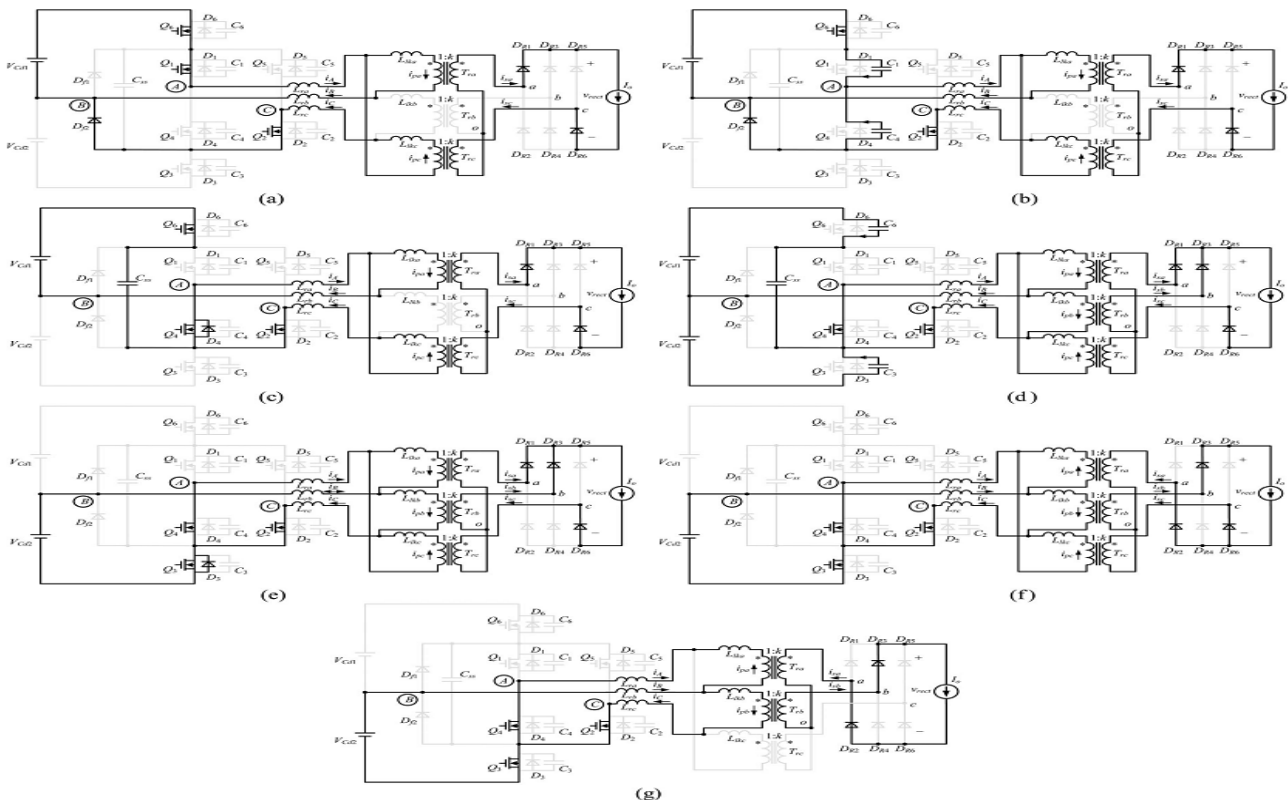


Fig. 4. Equivalent circuits under different operation stages. (a) Prior to t_0 , (b) $[t_0, t_1]$, (c) $[t_1, t_2]$, (d) $[t_2, t_3]$, (e) $[t_3, t_4]$, (f) $[t_4, t_5]$, (g) $[t_5, t_6]$.

Where $Z_r = \sqrt{L_p/C_p}$, $\omega_r = \sqrt{1/(L_p \cdot C_p)}$ and $L_p = L_{lk} + 3L_r$. During this stage, v_{rect} remains at zero. When v_{C3} decays to zero, D_3 conducts naturally.

Stage 5 $[t_3, t_4]$ [see Fig. 4(e)]: As D_3 is conducting, the voltage across Q_3 is clamped at zero; therefore, Q_3 is

turned on at zero-voltage condition. During this stage, Q_2 , Q_3 , and Q_4 conduct in the primary stage, $v_{AB}=-V_{in}/2$, $v_{BC}=V_{in}/2$, and $v_{CA}=0$. D_{R1} , D_{R3} , and D_{R6} conduct in the secondary stage, and $v_{rect}=0$. From (3.1), (3.2), (3.4), and other constraints between voltages and currents of transformers, the expressions of the phase currents are given in (3.14)–(3.16)

$$i_{pa}(t) = i_{pa}(t_3) - \frac{V_{in}}{2L_p} \cdot (t - t_3) \quad (14)$$

$$i_{pb}(t) = i_{pb}(t_3) + \frac{V_{in}}{2L_p} \cdot (t - t_3) \quad (15)$$

$$i_{pc}(t) = -kI_o \quad (16)$$

Stage 6 [t₄,t₅] [see Fig. 4(f)]: During this stage, v_{AB}=-V_{in}/2, v_{BC}=V_{in}/2, v_{CA}=0. From the constraints between voltages and currents of transformers, the following expressions can be obtained:

$$i_A(t) = k \cdot I_o - \frac{V_{in}}{2L_p} \cdot (t - t_4) \quad (17)$$

$$i_B(t) = k \cdot I_o + \frac{V_{in}}{4L_p} \cdot (t - t_4) \quad (18)$$

$$i_C(t) = -2k \cdot I_o + \frac{V_{in}}{4L_n} \cdot (t - t_4) \quad (19)$$

I_{sc} flows through D_{R6}, i_{sc} and decreases with i_{pc}. When i_{sc} decreases to zero, D_{R6} turns off, the primary and secondary currents of transformer T_{rc} are both zero. The time interval of this stage is given by

$$t_{45} = \frac{4k \cdot I_o \cdot L_p}{V_{in}} \quad (20)$$

Hereafter, Q₂, Q₃, and Q₄ conduct at the primary side, while DR₂ and DR₃ conduct at the secondary side, and the rectified voltage is k V_{in}, which is similar to the stage 1.

IV. THEORETICAL ANALYSIS

A. Input Capacitor Balancing Analysis

It has been known that by using PWM to control the converter, the input capacitor balancing is a function of the duty cycle and the charging/discharging current. If the symmetrical duty cycle control is utilized, each input capacitor presents one-half of the input voltage. While using an asymmetrical duty cycle control, an analysis of the input capacitor energy must be made. Fig. 5 shows the ideal charging/discharging waveforms for the input capacitor under different operation modes, in which the influence of the leakage inductance and the resonant inductance are omitted without detriment to the analysis. Table I presents the steady-state analysis of the input capacitors energy during the power transfer stages. In this analysis it is assumed that the load current is constant in a switching period. The symbol “↑” means that the capacitor is delivering energy,

therefore, its voltage is decreasing, while “↓” means that the capacitor is receiving energy and its voltage is increasing. From Fig. 5 and Table I, it can be seen that the capacitor C_{d1} is discharged in the interval ΔT₁ and is charged in the interval ΔT₂; here, ΔT₂=2ΔT₁ and the charging current is one-half of the discharging current. The opposite operation occurs in C_{d2}.

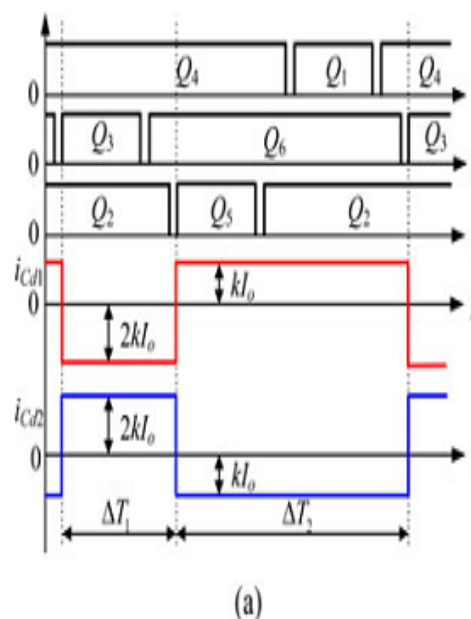
As a result, the total energy variations of input capacitors are equal to zero, considering that the amount of energy variations is equal in two intervals. Therefore, during a switching period the total voltage variation in each input capacitor is equal to zero, and all input capacitors voltages remain equal to one-half of the input voltage.

TABLE I
ENERGY BALANCE OF INPUT CAPACITORS UNDER DIFFERENT OPERATION MODES

Small duty cycle mode			Medium duty cycle mode		
Time interval	ΔT ₁	ΔT ₂	Time interval	ΔT ₁	ΔT ₂
C _{d1}	↑	↓	C _{d1}	↑	↓
C _{d2}	↓	↑	C _{d2}	↓	↑
Total energy	0	0	Total energy	0	0

B. Output Filter Inductance

With three-phase architecture, the converter with modified control strategy can reduce the output current ripple and further minimize the output filter requirement. Figs. 6 and 7 show the waveforms of the rectified voltage v_{rect} and the output filter inductance current i_{Lf} under SDCM and MDCM, respectively. From Figs. 6 and 7, the expressions of the output filter inductance are given in (3.31)



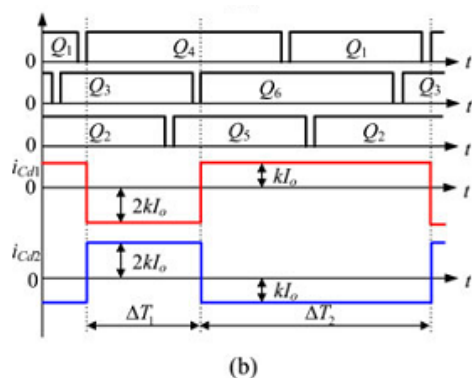


Fig. 5. Ideal charging/discharging waveforms under different operation modes. (a) SDCM. (b) MDCM.

$$L_{f_HB} = \frac{V_o \cdot (1 - 2V_o/k_{HB} \cdot V_{in})}{2\Delta i_{L_f} \cdot f_s} \quad (21)$$

Where k_{HB} is the turns ratio of the transformer in half-bridge TL converter, $k_{HB}=4V_o/(V_{inmin} \cdot D_{HBmax})$, and D_{HBmax} is the maximum duty cycle that is set at 0.45. Fig. 8 shows quantitatively the savings in the inductance requirement as a function of the range of input variation, and the Y-coordinate is the ratio of L_f TP to the maximum L_f HB, where input voltage $V_{in} = 540-660$ V, output voltage $V_o=48$ V, output current $I_o = 20$ A, switching frequency $f_s = 50$ kHz, and $\Delta i_{L_f} = 4$ A. As shown, the TPTL converter with modified control scheme can save the output filter inductance effectively, which is reduced by a factor of about 52% compared with the half-bridge TL converter.

D. Current Stress and Voltage Stress on Switches

To demonstrate the reduction of current stress on switches under the modified control strategy, the ideal current waveforms of switches in different operation modes are illustrated in Fig. 9, in which the leakage inductance and the current ripple of output filter inductance are neglected. From Fig. 9, the rms current through the switches I_{rms} under rated load are given by

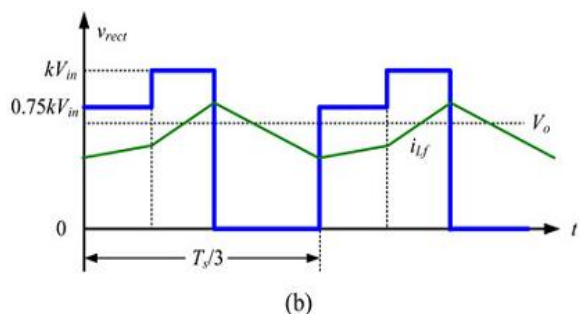
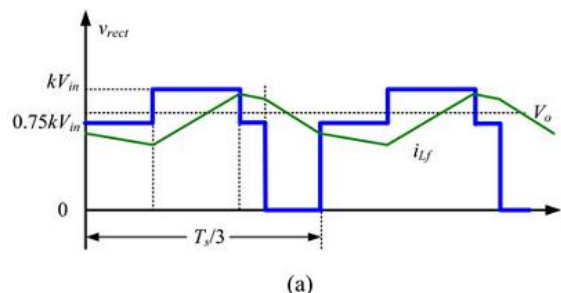
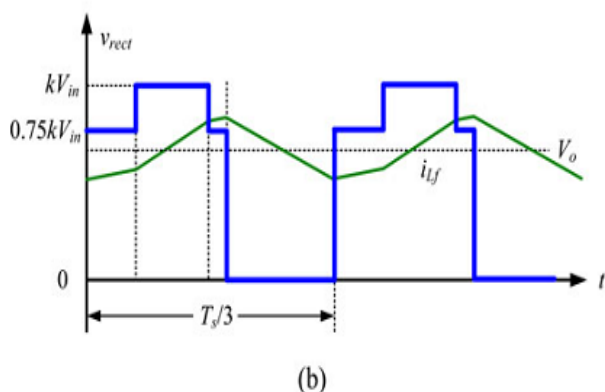


Fig. 6. Waveforms of the rectified voltage and output filter inductance current under SDCM. (a) $0.75kV_{in} < V_o < kV_{in}$. (b) $V_o < 0.75kV_{in}$



(a)



(b)

Fig.7. Waveforms of the rectified voltage and output filter inductance current under MDCM. (a) $0.75kV_{in} < V_o < kV_{in}$. (b) $V_o < 0.75kV_{in}$.

To illustrate the good performance of the proposed converter, the half-bridge TL converter is adopted to make the comparison. The output filter inductance of half-bridge TL converter is

$$I_{rms_Q1} = \begin{cases} k \cdot I_o \cdot \sqrt{4D - D_{loss1}} & \text{(SDCM)} \\ k \cdot I_o \cdot \sqrt{1 + D - D_{loss2}} & \text{(MDCM)} \end{cases} \quad (22)$$

$$I_{rms_Q4} = \begin{cases} k \cdot I_o \cdot \sqrt{2 - 4D + D_{loss1}} & \text{(SDCM)} \\ k \cdot I_o \cdot \sqrt{1 - D + D_{loss2}} & \text{(MDCM)} \end{cases} \quad (23)$$

Likewise, the half-bridge TL converter could be used for comparison. If the phase-shifted control is employed, the rms current through the switches will be given by

$$I_{rms_HB} = k_{HB} \cdot I_o \cdot \sqrt{\frac{1}{2}} \quad (24)$$

Using the specifications given previously, Fig. 10 illustrates quantitatively the savings in the rms current through switches as a function of input variation range, and the Y-coordinate is the ratio of I_{rms} to the I_{rms} HB. As shown, the rms current through power switches can be reduced compared with the half bridge TL converter, which means that the switches can sustain higher power in the modified TPTL converter. Meanwhile, the two complementary switches suffer different current stresses due to the asymmetrical duty cycle, and it should be considered in the practical design.

As for the voltage ratings on switches, thanking for the TL configuration and the automatic voltage balancing

of input capacitors, the voltage stress on power switches will be limited at half of the input voltage, so the converter is suitable for high input voltage applications.

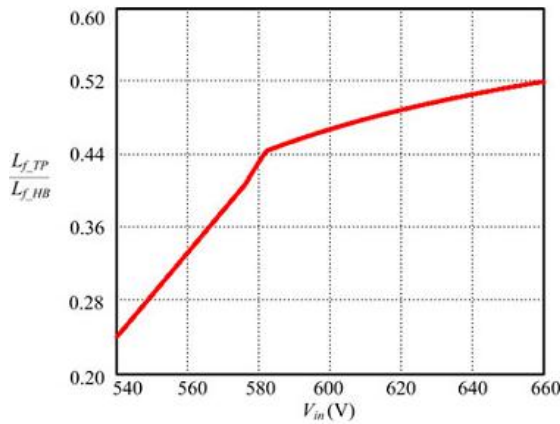


Fig.8. Ratio of L_{f_TP} and L_{f_HB} versus the input voltage

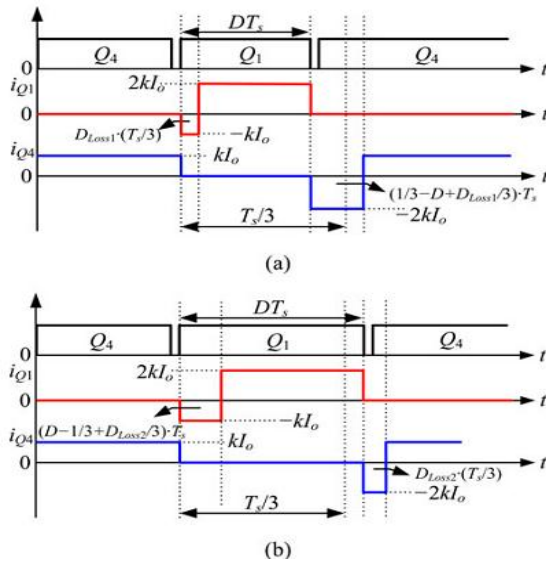


Fig.9. Ideal current waveforms of switches. (a) SDCM. (b) MDCM

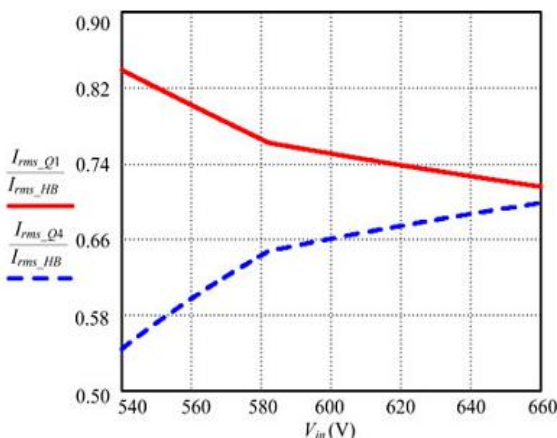


Fig. 10. Ratio of I_{rms_Q1} and I_{rms_Q4} versus the input voltage

E. Conditions for Soft-Switching Realization

In order to achieve ZVS for the switches, enough energy is needed to fully charge/discharge the intrinsic capacitors of the switches prior to turning on the switches. Due to the different operation principles in two modes, the converter presents different ZVS characteristics. 1) SDCM: During the transition of Q_2 , Q_4 , and Q_6 , as seen in Fig. 3(a), the charging currents for the intrinsic capacitors are proportional to the reflected load current, thus the voltage across the switches varies linearly, and the energy to achieve ZVS for the three switches is provided by the output filter inductance. To ensure zero-voltage turn-on, the intrinsic capacitor of the incoming switch should be fully discharged by the line current during the delay time. From (8), it can be known that the ZVS condition will be lost if the load current is below $I_{o_min_Q2(Q4,Q6)}$ expressed by

$$I_{o_min_Q2(Q4,Q6)} = \frac{V_{in} \cdot C_p}{2t_d \cdot k} \quad (25)$$

During the commutation Q_1 , Q_3 , and Q_5 , the resonant inductances and the leakage inductances resonate with the intrinsic capacitors of these switches, and only the energy stored in the resonant inductances and the leakage inductances are used to achieve zero-voltage turn-on. From (3.9) and (3.10), the minimum load current to realize ZVS for Q_1 , Q_3 , and Q_5 is given by

$$I_{o_min_Q1(Q3,Q5)} = \frac{V_{in}}{Z_r \cdot k} \quad (26)$$

The minimum load current to achieve ZVS under SDCM as the function of the input voltage is depicted in Fig. 11, from which we can see that Q_2, Q_4 , and Q_6 can realize ZVS easier compared with Q_1, Q_3 , and Q_5 , and the ZVS load range for Q_1, Q_3 , and Q_5 can be widened by increasing the resonant inductances.

2) MDCM: Similarly, from Fig. 3(b), the minimum load currents to achieve ZVS for switches under MDCM are given by

$$I_{o_min_Q1(Q3,Q5)} = \frac{V_{in} \cdot C_p}{t_d \cdot k} \quad (27)$$

$$I_{o_min_Q2(Q4,Q6)} = \frac{\sqrt{3}V_{in}}{4Z_{r1} \cdot k} \quad (28)$$

where $Z_{r1} = \sqrt{L_v / 4C_d}$

It should be noted that the critical point between SDCM and MDCM depends on the duty cycle and the load current according to (3.30). Substituting $D=1/3$ into the second expression in (3.30), the minimum load current

that ensures the converter to operate under MDCM is given by

$$I_{o_min} = \frac{k \cdot V_{in} - V_o}{9k^2 \cdot L_p \cdot f_s} \quad (29)$$

Fig. 4.12 illustrates the minimum load currents in (38)–(40) as a function of the input voltage, which indicates that the switches can realize ZVS within the operation range in MDCM, considering the minimum load current to satisfy the requirement of MDCM is larger than the minimum load current to achieve ZVS

F. Considerations on Dynamic Behavior of Modified Converter

The modified TPTL converter has almost the same problems to closing the feedback loop as the asymmetrical half-bridge converters. The phase lag caused by the double pole–double zero of the transfer function can cause stability problems, for the phase margin is small or even null under some loads. In the practical design, the following considerations should be emphasized to achieve a better dynamic performance: 1) Combination of multilayer capacitors in parallel with electrolytic capacitors in the input capacitor design. The combination of both type of capacitor can dump the effect of the double-pole double-zero effectively. 2) A lead–lag controller should be introduced into the closed-loop design, which put both zeros of the lead–lag controller at a frequency below the double-pole frequency. Thus, the phase margin at the frequencies near the double pole–double zero effect is quite large. With the lead–lag controller, the modified converter can achieve a larger phase margin and a higher band-width than that with a single PI controller, which will be favorable to obtain a more stable steady behavior and a faster dynamic response.

Proposed Concept with 5 level converter:

The 5 level converter reduces the harmonics, when it was first used in a three-level converter in which the mid-voltage level was defined as the neutral point. The 5 level converter uses capacitors in series to divide up the dc bus voltage into a set of voltage levels. To produce m levels of the phase voltage, an m level 5 level converter needs m-1 capacitors on the dc bus. A single-phase five-level converter is shown in Fig. 1.9. The dc bus consists of four capacitors, i.e., C1, C2, C3, and C4. For a dc bus voltage V_{dc} , the voltage across each capacitor is $V_{dc}/4$, and each device voltage stress will be limited to one capacitor voltage level, $V_{dc}/4$, through clamping diodes. DCMI output voltage synthesis is relatively straightforward.

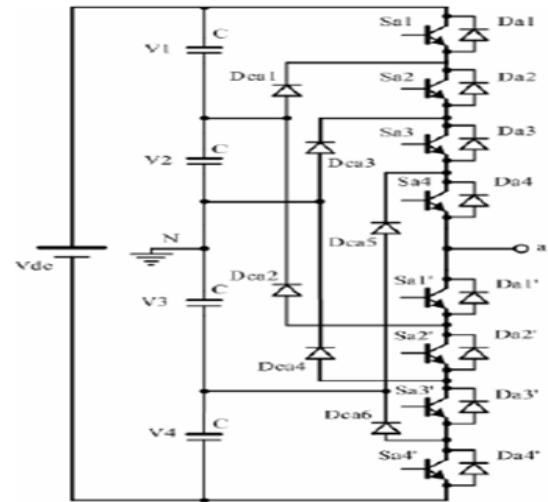


Fig.11.Five level converter

To explain how the staircase voltage is synthesized, point O is considered as the output phase voltage reference point. Using the five-level converter shown in Fig. 1.10, there are five switch combinations to generate five level voltage level and their corresponding switch states. From Table 2.2, state 1 represents that the switch is on, and state 0 represents the switch is off. In each phase leg, a set of four adjacent switches is on at any given time. There exist four complimentary switch pairs in each phase, i.e., Sa1-Sa1', Sa2-Sa2', and Sa4-Sa4'.

Table II: five-level converter voltage levels and their switch states

Output V_{AO}	Switch state							
	S_{a1}	S_{a2}	S_{a3}	S_{a4}	$S_{a1'}$	$S_{a2'}$	$S_{a3'}$	$S_{a4'}$
$V_5=V_{dc}$	1	1	1	1	0	0	0	0
$V_4=3V_{dc}/4$	0	1	1	1	1	0	0	0
$V_3=V_{dc}/2$	0	0	1	1	1	1	0	0
$V_2=V_{dc}/4$	0	0	0	1	1	1	1	0
$V_1=0$	0	0	0	0	1	1	1	1

V. MATLAB/SIMULINK RESULTS

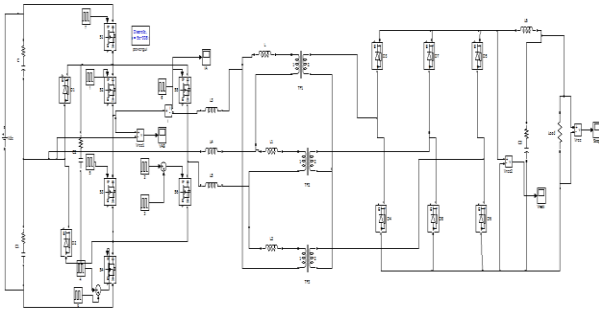


Fig.12.Simulation result for TPTL dc/dc converter

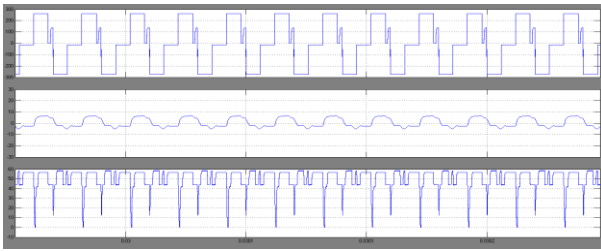


Fig.13.Simulation result for V_{ab} , I_a , V_{rect} at medium duty cycle mode (MDCM)

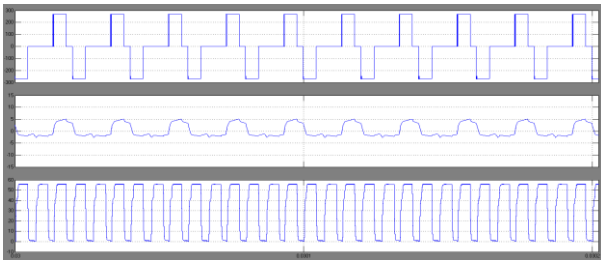


Fig.17.Simulation result for gate signal, V_{ds} and I_d for Q2 for SDCM

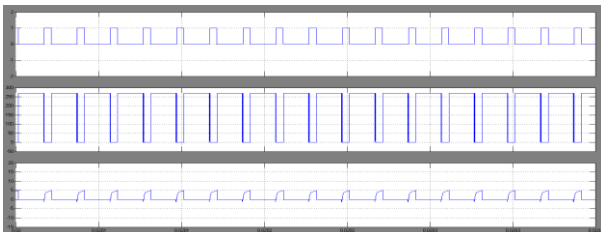


Fig.18.Simulation result for gate signal, V_{ds} and I_d for Q5 for SDCM

Fig.14.Simulation result for V_{ab} , I_a , V_{rect} at small duty cycle mode (SDCM)

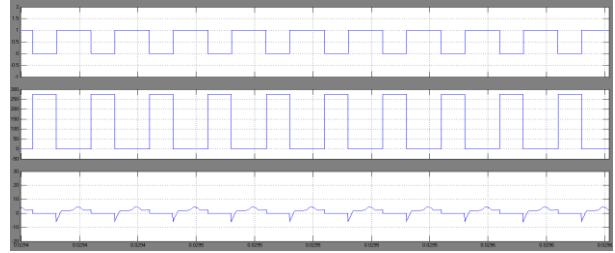


Fig.15.Simulation result for gate signal, V_{ds} and I_d for Q2 for MDCM

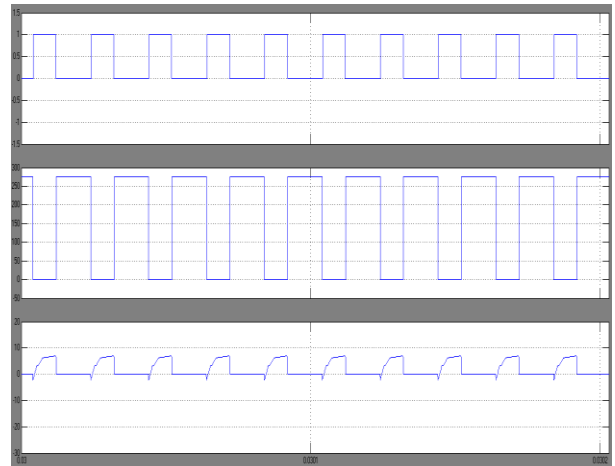


Fig.16.Simulation result for gate signal, V_{ds} and I_d for Q5 for MDCM

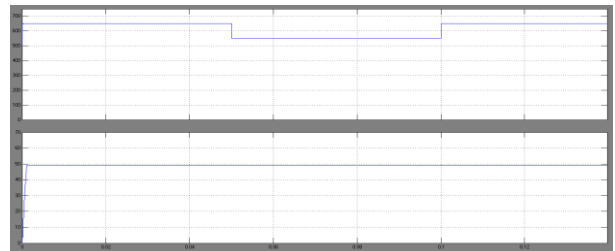


Fig.19.Simulation result for input and output voltage during step change in voltage

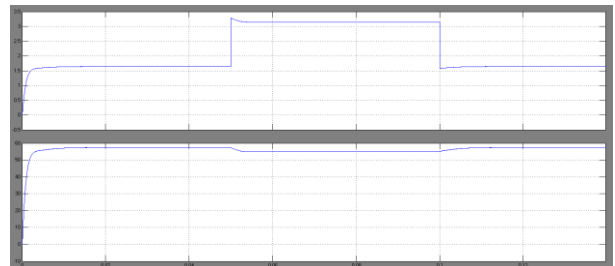


Fig.20. Simulation result for input and output voltage during step change in current

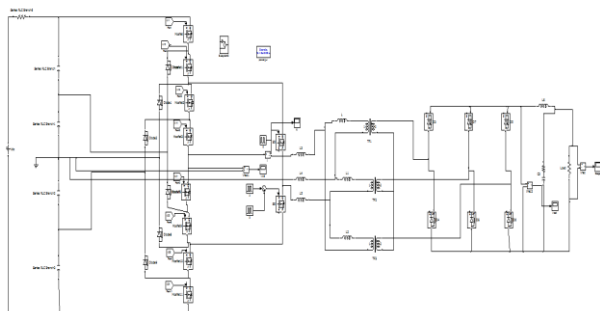


Fig.21.Simulink design for five level converter

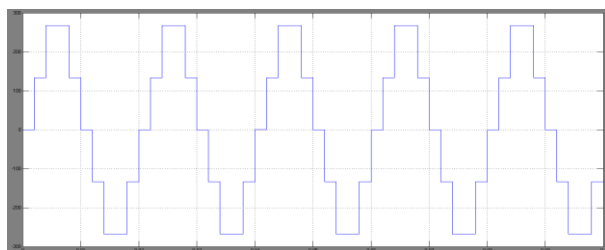


Fig.22.Simulation result for five level converter

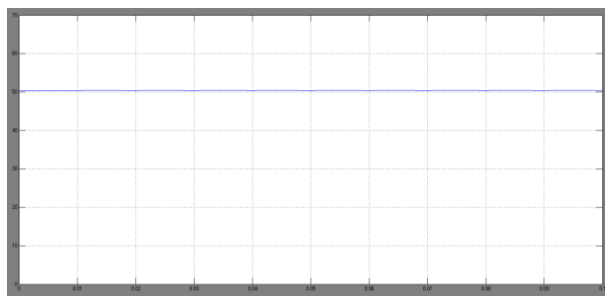


Fig.23.Simulation result for output voltage

VI. CONCLUSION

A modified asymmetrical duty cycle control strategy with ZVS capability was proposed for the TPTL converter in this paper. The proposed control scheme features are- Compared with the symmetrical duty cycle control, the dominant advantages can be maintained including the lower power rating of switches and the reduced output filter requirement. The input capacitors can realize automatic and inherent voltage balancing, which ensures that all the switches sustain only one-half of the input voltage. The TPTL converter will operate in three operation modes along with the variation of duty cycle and output current, i.e., SDCM, MDCM in which, the output voltage cannot be modulated under LDCM. Three level converter has higher harmonic order so we replaced with five level converter for reduction of harmonics.

REFERENCES

[1] R. W. De Doncker, D. M. Divan, and M. H. Kheraluwala, "A three phase soft-switched high-power-density DC/DC converter for high-power applications," *IEEE Trans. Ind. Appl.*, vol. 27, no. 1, pp. 63–73, Jan./Feb. 1991.

[2] H. Cha and P. Enjeti, "A novel three-phase high power current-fed DC/DC converter with active clamp for fuel cells," in *Proc. IEEE Power Electron. Spec. Conf.*, 2007, pp. 2485–2489.

[3] A. Sunil, G. E. Michael, and J. W. Michael, "Analysis and design of a new three-phase LCC-type resonant DC–DC converter with capacitor output filter," in *Proc. IEEE Power Electron. Spec. Conf.*, 2000, pp. 721–728.

[4] M. Almardy and A. K. S. Bhat, "Three-phase (LC)(L)-type series resonant converter with capacitive output filter," in *Proc. IEEE Int. Conf. Power Electron. Drive Syst.*, 2007, pp. 468–475.

[5] M. Almardy and A. K. S. Bhat, "Three-phase (LC)(L)-type seriesresonant converter: Design and experimental results," in *Proc. Int. Conf. Electron. Devices, Syst. Appl.*, 2010, pp. 70–75.

[6] D. S. Oliveira, Jr and I. Barbi, "A three-phase ZVS PWM DC/DC converter with asymmetrical duty cycle associated with a three-phase version of the hybrid rectifier," *IEEE Trans. Power Electron.*, vol. 20, no. 2, pp. 354–360, Mar. 2005.

[7] T. Song, N. Huang, and A. Ioinovici, "Zero-voltage and zero-current switching three-level DC–DC converter with reduced rectifier voltage stress and soft-switching-oriented optimized design," *IEEE Trans. Power Electron.*, vol. 21, no. 5, pp. 1204–1212, Sep. 2006.

[8] J. A. Carr, B. Rowden, and J. C. Balda, "A three-level full-bridge zero-voltage zero-current switching converter with a simplified switching scheme," *IEEE Trans. Power Electron.*, vol. 24, no. 2, pp. 329–338, Feb. 2009.

[9] D. V. Ghodke, K. Chatterjee, and B. G. Fernandes, "Three-phase three level, soft switched, phase shifted PWM dc-dc converter for high power applications," *IEEE Trans. Power Electron.*, vol. 23, no. 3, pp. 1214–1227, May 2008.

[10] D. V. Ghodke, K. Chatterjee, and B. G. Fernandes, "Modified soft switched three-phase three-level DC–DC converter for high-power applications having extended duty cycle range," *IEEE Trans. Ind. Electron.*, vol. 59, no. 9, pp. 3362–3372, Sep. 2012.

[11] F. Liu, G. Hu, and X. Ruan, "Three-phase three-level DC/DC converter for high input voltage and high-power applications-adopting symmetrical duty cycle control," *IEEE Trans. Power Electron.*, vol. 29, no. 1, pp. 56–65, Jan. 2014.

[12] H. Kim, C. Yoon, and S. Choi, "A three-phase DC–DC converter for fuel cell applications," in *Proc. IEEE Power Electron. Spec. Conf.*, 2008, pp. 1290–1295.